PHYSICAL REVIEW D **90,** 052011 (2014)

Measurement of *CP* violation in $B_s^0 \to \phi\phi$ decays

R. Aaij *et al.*[*]
(LHCb Collaboration)

(Received 8 July 2014; published 30 September 2014)

A measurement of the decay time-dependent *CP*-violating asymmetry in $B_s^0 \to \phi\phi$ decays is presented, along with measurements of the *T*-odd triple-product asymmetries. In this decay channel, the *CP*-violating weak phase arises from the interference between B_s^0-$\bar{B}_s^0$ mixing and the loop-induced decay amplitude. Using a sample of proton-proton collision data corresponding to an integrated luminosity of 3.0 fb^{-1} collected with the LHCb detector, a signal yield of approximately 4000 $B_s^0 \to \phi\phi$ decays is obtained. The *CP*-violating phase is measured to be $\phi_s = -0.17 \pm 0.15(\text{stat}) \pm 0.03(\text{syst})$ rad. The triple-product asymmetries are measured to be $A_U = -0.003 \pm 0.017(\text{stat}) \pm 0.006(\text{syst})$ and $A_V = -0.017 \pm 0.017(\text{stat}) \pm 0.006(\text{syst})$. Results are consistent with the hypothesis of *CP* conservation.

DOI: 10.1103/PhysRevD.90.052011 PACS numbers: 13.25.Hw, 11.30.Er, 12.15.Hh, 14.40.Nd

I. INTRODUCTION

The $B_s^0 \to \phi\phi$ decay is forbidden at tree level in the Standard Model (SM) and proceeds predominantly via a gluonic $\bar{b} \to \bar{s}s\bar{s}$ loop (penguin) process. Hence, this channel provides an excellent probe of new heavy particles entering the penguin quantum loops [1–3]. In the SM, *CP* violation is governed by a single phase in the Cabibbo–Kobayashi–Maskawa quark mixing matrix [4]. Interference between the B_s^0-$\bar{B}_s^0$ oscillation and decay amplitudes leads to a *CP* asymmetry in the decay time distributions of B_s^0 and $\bar{B}_s^0$ mesons, which is characterized by a *CP*-violating weak phase. Because of different decay amplitudes the actual value of the weak phase is dependent on the B_s^0 decay channel. For $B_s^0 \to J/\psi K^+K^-$ and $B_s^0 \to J/\psi\pi^+\pi^-$ decays, which proceed via $\bar{b} \to \bar{s}c\bar{c}$ transitions, the SM prediction of the weak phase is given by $-2\ \arg(-V_{ts}V_{tb}^*/V_{cs}V_{cb}^*) = -0.0364 \pm 0.0016$ rad [5]. The LHCb collaboration has measured the weak phase in the combination of $B_s^0 \to J/\psi K^+K^-$ and $B_s^0 \to J/\psi\pi^+\pi^-$ decays to be $0.07 \pm 0.09(\text{stat}) \pm 0.01(\text{syst})$ rad [6]. A recent analysis of $B_s^0 \to J/\psi\pi^+\pi^-$ decays using the full LHCb run I data set of 3.0 fb^{-1} has measured the *CP*-violating phase to be $0.070 \pm 0.068(\text{stat}) \pm 0.008(\text{syst})$ rad [7]. These measurements are consistent with the SM and place stringent constraints on *CP* violation in B_s^0-$\bar{B}_s^0$ oscillations [8]. The *CP*-violating phase, ϕ_s, in the $B_s^0 \to \phi\phi$ decay is expected to be small in the SM. Calculations using quantum chromodynamics factorization (QCDf) provide an upper limit of 0.02 rad for $|\phi_s|$ [1–3].

Triple-product asymmetries are formed from *T*-odd combinations of the momenta of the final-state particles. Such asymmetries provide a method of measuring *CP* violation in a decay time integrated method that complements the decay time-dependent measurement [9]. These asymmetries are calculated from functions of the angular observables and are expected to be close to zero in the SM [10]. Particle-antiparticle oscillations reduce nonzero triple-product asymmetries due to *CP*-conserving strong phases, known as "fake" triple-product asymmetries by a factor $\Gamma/(\Delta m)$, where Γ and Δm are the decay rates and oscillation frequencies of the neutral meson system in question. Since one has $\Gamma_s/(\Delta m_s) \approx 0.04$ for the B_s^0 system, fake triple-product asymmetries are strongly suppressed, allowing for "true" *CP*-violating triple-product asymmetries to be calculated without the need to measure the initial flavor of the B_s^0 meson [9].

Theoretical calculations can be tested further with measurements of the polarization fractions, where the longitudinal and transverse polarization fractions are denoted by f_L and f_T, respectively. In the heavy quark limit, f_L is expected to be the dominant polarization due to the vector-axial structure of charged weak currents [2]. This is found to be the case for tree-level *B* decays measured at the *B* factories [11–16]. However, the dynamics of penguin transitions are more complicated. In the context of QCDf, f_L is predicted to be $0.36^{+0.23}_{-0.18}$ for the $B_s^0 \to \phi\phi$ decay [3].

In this paper, a measurement of the *CP*-violating phase in $B_s^0 \to \phi(\to K^+K^-)\phi(\to K^+K^-)$ decays, along with a measurement of the *T*-odd triple-product asymmetries, is presented. The results are based on pp collision data corresponding to an integrated luminosity of 1.0 fb^{-1} and 2.0 fb^{-1} collected by the LHCb experiment at center-of-mass energies $\sqrt{s} = 7$ TeV in 2011 and 8 TeV in 2012, respectively. Previous measurements of the triple-product asymmetries from the LHCb [17] and CDF [18] collaborations, together with the first measurement of the

[*] Full author list given at the end of the article.

CP-violating phase in $B_s^0 \to \phi\phi$ decays [17], have shown no evidence of deviations from the SM. The decay time-dependent measurement improves on the previous analysis [17] through the use of a more efficient candidate selection and improved knowledge of the B_s^0 flavor at production, in addition to a data-driven determination of the efficiency as a function of decay time.

The results presented in this paper supersede previous measurements of the CP-violating phase [17] and T-odd triple-product asymmetries [19], made using 1.0 fb^{-1} of data collected at a $\sqrt{s} = 7$ TeV.

II. DETECTOR DESCRIPTION

The LHCb detector [20] is a single-arm forward spectrometer covering the pseudorapidity range $2 < \eta < 5$, designed for the study of particles containing b or c quarks. The detector includes a high-precision tracking system consisting of a silicon-strip vertex detector surrounding the pp interaction region, a large-area silicon-strip detector located upstream of a dipole magnet with a bending power of about 4 Tm, and three stations of silicon-strip detectors and straw drift tubes [21] placed downstream. The combined tracking system provides a momentum measurement with relative uncertainty that varies from 0.4% at low momentum to 0.6% at 100 GeV/c and impact parameter resolution of 20 μm for tracks with large transverse momentum, p_{T}. Different types of charged hadrons are distinguished using information from two ring-imaging Cherenkov (RICH) detectors [22]. Photon, electron, and hadron candidates are identified by a calorimeter system consisting of scintillating-pad and preshower detectors, an electromagnetic calorimeter, and a hadronic calorimeter. The trigger [23] consists of a hardware stage, based on information from the calorimeter and muon systems, followed by a software stage, which applies a full event reconstruction. The hardware trigger selects $B_s^0 \to \phi\phi$ candidates by requiring large transverse energy deposits in the calorimeters from at least one of the final-state particles. In the software trigger, $B_s^0 \to \phi\phi$ candidates are selected either by identifying events containing a pair of oppositely charged kaons with an invariant mass close to that of the ϕ meson or by using a topological b-hadron trigger. The topological software trigger requires a two-, three-, or four-track secondary vertex with a large sum of the p_{T} of the charged particles and a significant displacement from the primary pp interaction vertices (PVs). At least one charged particle should have $p_{\mathrm{T}} > 1.7$ GeV/c and χ^2_{IP} with respect to any primary interaction greater than 16, where χ^2_{IP} is defined as the difference in χ^2 of a given PV fitted with and without the considered track. A multivariate algorithm [24] is used for the identification of secondary vertices consistent with the decay of a b-hadron.

In the simulation, pp collisions are generated using PYTHIA [25] with a specific LHCb configuration [26]. Decays of hadronic particles are described by EVTGEN [27], in which final-state radiation is generated using PHOTOS [28]. The interaction of the generated particles with the detector and its response are implemented using the GEANT4 toolkit [29] as described in Ref. [30].

III. SELECTION AND MASS MODEL

Events passing the trigger are initially required to pass loose requirements on the fit quality of the four-kaon vertex fit, the χ^2_{IP} of each track, the transverse momentum of each particle, and the product of the transverse momenta of the two ϕ candidates. In addition, the reconstructed mass of ϕ meson candidates is required to be within 25 MeV/c^2 of the known ϕ mass [31].

To further separate the $B_s^0 \to \phi\phi$ signal from the background, a boosted decision tree (BDT) is implemented [32,33]. To train the BDT, simulated $B_s^0 \to \phi\phi$ events passing the same loose requirements as the data events are used as signal, whereas events in the four-kaon invariant mass sidebands from data are used as background. The signal mass region is defined to be less than 120 MeV/c^2 from the known B_s^0 mass, $m_{B_s^0}$ [31]. The invariant mass sidebands are defined to be inside the region $120 < |m_{K^+K^-K^+K^-} - m_{B_s^0}| < 300$ MeV/c^2, where $m_{K^+K^-K^+K^-}$ is the four-kaon invariant mass. Separate BDTs are trained for data samples collected in 2011 and 2012, due to different data taking conditions in the different years. Variables used in the BDT consist of the minimum and maximum kaon p_{T} and η, the minimum and the maximum p_{T} and η of the ϕ candidates, the p_{T} and η of the B_s^0 candidate, the minimum probability of the kaon mass hypothesis using information from the RICH detectors, the quality of the four-kaon vertex fit, and the χ^2_{IP} of the B_s^0 candidate. The BDT also includes kaon isolation asymmetries. The isolation variable is calculated as the scalar sum of the p_{T} of charged particles inside a region defined as $\sqrt{\Delta\varphi^2 + \Delta\eta^2} < 1$, where $\Delta\varphi(\Delta\eta)$ is the difference in azimuthal angle (pseudorapidity), not including the signal kaon from the B_s^0 decay. The asymmetry is then calculated as the difference between the isolation variable and the p_{T} of the signal kaon, divided by the sum. After the BDT is trained, the optimum requirement on each BDT is chosen to maximize $N_{\mathrm{S}}/\sqrt{N_{\mathrm{S}} + N_{\mathrm{B}}}$, where $N_{\mathrm{S}}(N_{\mathrm{B}})$ represent the expected number of signal (background) events in the signal region of the data sample.

The presence of peaking backgrounds is extensively studied. The decay modes considered include $B^+ \to \phi K^+$, $B^0 \to \phi\pi^+\pi^-$, $B^0 \to \phi K^{*0}$, and $\Lambda_b^0 \to \phi p K^-$, of which only the last two are found to contribute and are the result of a misidentification of a pion or proton as a kaon, respectively. The number of $B^0 \to \phi K^{*0}$ events present in the data sample is determined from scaling the number of $B^0 \to \phi K^{*0}$ events seen in data through a different dedicated selection with the relative efficiencies between the two selections found from simulated events. This

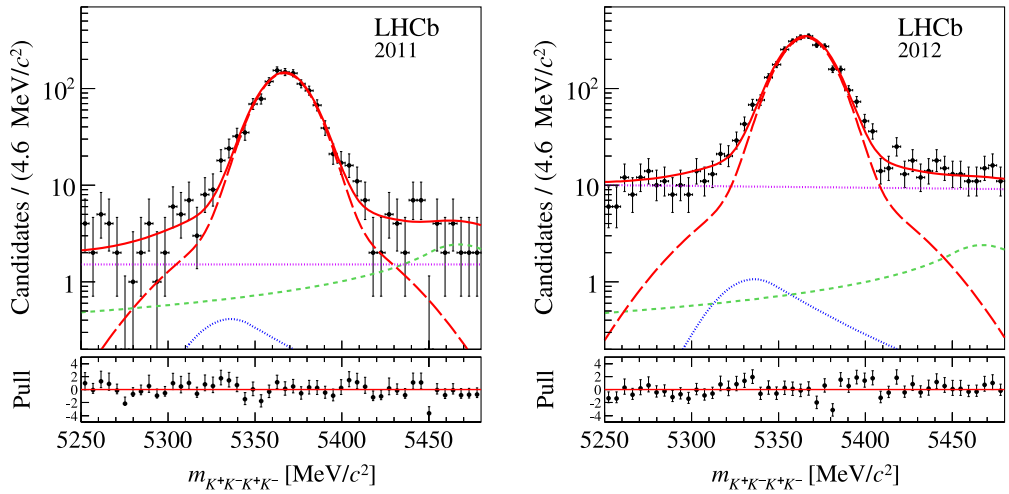

FIG. 1 (color online). Four-kaon invariant mass distributions for the (left) 2011 and (right) 2012 data sets. The data points are represented by the black markers. Superimposed are the results of the total fit (red solid line), the $B_s^0 \to \phi\phi$ (red long dashed), the $B^0 \to \phi K^{*0}$ (blue dotted), the $\Lambda_b^0 \to \phi p K^-$ (green short-dashed), and the combinatoric (purple dotted) fit components.

method yields values of 7.3 ± 0.4 and 17.8 ± 0.9 events in the 2011 and 2012 data sets, respectively. The amount of $\Lambda_b^0 \to \phi p K^-$ decays is estimated directly from data by changing the mass hypothesis of the final-state particle most likely to have the mass of the proton from RICH detector information. This method yields 52 ± 19 and 51 ± 29 $\Lambda_b^0 \to \phi p K^-$ events in the 2011 and 2012 data sets, respectively.

To correctly determine the number of $B_s^0 \to \phi\phi$ events in the final data sample, the four-kaon invariant mass distributions are fitted with the $B_s^0 \to \phi\phi$ signal described by a double Gaussian model and the combinatorial background component described using an exponential function. The peaking background contributions are fixed to the shapes found in simulated events. The yields of the peaking background contributions are fixed to the numbers previously stated. This consists of the sum of a Crystal Ball function [34] and a Gaussian to describe the $B^0 \to \phi K^{*0}$ reflection and a Crystal Ball function to describe the $\Lambda_b^0 \to \phi p K^-$ reflection. Once the BDT requirements are imposed, an unbinned extended maximum likelihood fit to the four-kaon invariant mass yields 1185 ± 35 and 2765 ± 57 $B_s^0 \to \phi\phi$ events in the 2011 and 2012 data sets, respectively. The combinatorial background yield is found to be 76 ± 17 and 477 ± 32 in the 2011 and 2012 data sets, respectively. The fits to the four-kaon invariant mass are shown in Fig. 1.

The use of the four-kaon invariant mass to assign signal weights allows for a decay time-dependent fit to be performed with only the signal distribution explicitly described. The method for assigning the signal weights is described in greater detail in Sec. VIII A.

IV. PHENOMENOLOGY

The $B_s^0 \to \phi\phi$ decay is composed of a mixture of *CP* eigenstates, that are disentangled by means of an angular analysis in the helicity basis, defined in Fig. 2.

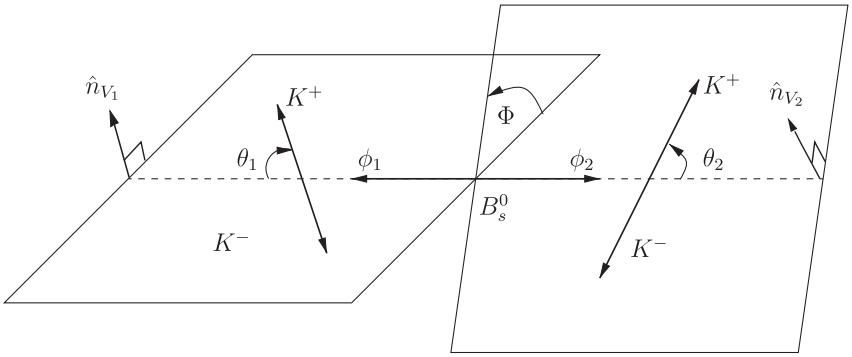

FIG. 2. Decay angles for the $B_s^0 \to \phi\phi$ decay, where the K^+ momentum in the $\phi_{1,2}$ rest frame and the parent $\phi_{1,2}$ momentum in the rest frame of the B_s^0 meson span the two ϕ meson decay planes, $\theta_{1,2}$ is the angle between the K^+ track momentum in the $\phi_{1,2}$ meson rest frame and the parent $\phi_{1,2}$ momentum in the B_s^0 rest frame, Φ is the angle between the two ϕ meson decay planes, and $\hat{n}_{V_{1,2}}$ is the unit vector normal to the decay plane of the $\phi_{1,2}$ meson.

A. Decay time-dependent model

The $B_s^0 \to \phi\phi$ decay is a $P \to VV$ decay, where P denotes a pseudoscalar and V a vector meson. However, due to the proximity of the ϕ resonance to that of the $f_0(980)$, there will also be contributions from S-wave ($P \to VS$) and double S-wave ($P \to SS$) processes, where S denotes a spin-0 meson or a pair of nonresonant kaons. Thus, the total amplitude is a coherent sum of P-, S-, and double S-wave processes and is accounted for during fitting by making use of the different functions of the helicity angles associated with these terms. The choice of which ϕ meson is used to determine θ_1 and which is used to determine θ_2 is randomized. The total amplitude ($\mathcal{A}$) containing the P-, S-, and double S-wave components as a function of decay time, t, can be written as [35]

$$\begin{aligned}\mathcal{A}(t,\theta_1,\theta_2,\Phi) = {} & A_0(t)\cos\theta_1\cos\theta_2 \\ & + \frac{A_\parallel(t)}{\sqrt{2}}\sin\theta_1\sin\theta_2\cos\Phi \\ & + i\frac{A_\perp(t)}{\sqrt{2}}\sin\theta_1\sin\theta_2\sin\Phi \\ & + \frac{A_S(t)}{\sqrt{3}}(\cos\theta_1+\cos\theta_2) + \frac{A_{SS}(t)}{3}, \quad (1)\end{aligned}$$

where A_0, $A_\parallel$, and $A_\perp$ are the CP-even longitudinal, CP-even parallel, and CP-odd perpendicular polarizations of the $B_s^0 \to \phi\phi$ decay. The $P \to VS$ and $P \to SS$ processes are described by the A_S and A_{SS} amplitudes, respectively. The differential decay rate may be found through the square of the total amplitude leading to the 15 terms [35]

$$\begin{aligned}\frac{d\Gamma}{dt\,d\cos\theta_1\,d\cos\theta_2\,d\Phi} & \propto 4|\mathcal{A}(t,\theta_1,\theta_2,\Phi)|^2 \\ & = \sum_{i=1}^{15} K_i(t) f_i(\theta_1,\theta_2,\Phi). \quad (2)\end{aligned}$$

The $K_i(t)$ term can be written as

$$\begin{aligned}K_i(t) = N_i e^{-\Gamma_s t}\Big[& c_i\cos(\Delta m_s t) + d_i\sin(\Delta m_s t) \\ & + a_i\cosh\left(\frac{1}{2}\Delta\Gamma_s t\right) + b_i\sinh\left(\frac{1}{2}\Delta\Gamma_s t\right)\Big], \quad (3)\end{aligned}$$

where the coefficients are shown in Table I, $\Delta\Gamma_s \equiv \Gamma_L - \Gamma_H$ is the decay width difference between the light and heavy B_s^0 mass eigenstates, $\Gamma_s \equiv (\Gamma_L + \Gamma_H)/2$ is the average decay width, and Δm_s is the B_s^0-$\bar{B}_s^0$ oscillation frequency. The differential decay rate for a $\bar{B}_s^0$ meson produced at $t = 0$ is obtained by changing the sign of the c_i and d_i coefficients.

The three CP-violating terms introduced in Table I are defined as

$$C \equiv \frac{1-|\lambda|^2}{1+|\lambda|^2}, \quad (4)$$

$$S \equiv -\frac{2|\lambda|\sin\phi_s}{1+|\lambda|^2}, \quad (5)$$

$$D \equiv -\frac{2|\lambda|\cos\phi_s}{1+|\lambda|^2}, \quad (6)$$

TABLE I. Coefficients of the time-dependent terms and angular functions used in Eq. (2). Amplitudes are defined at $t = 0$.

i	N_i	a_i	b_i	c_i	d_i	f_i
1	$\lvert A_0\rvert^2$	1	D	C	$-S$	$4\cos^2\theta_1\cos^2\theta_2$
2	$\lvert A_\parallel\rvert^2$	1	D	C	$-S$	$\sin^2\theta_1\sin^2\theta_2(1+\cos 2\Phi)$
3	$\lvert A_\perp\rvert^2$	1	$-D$	C	S	$\sin^2\theta_1\sin^2\theta_2(1-\cos 2\Phi)$
4	$\lvert A_\parallel\rvert\lvert A_\perp\rvert$	$C\sin\delta_1$	$S\cos\delta_1$	$\sin\delta_1$	$D\cos\delta_1$	$-2\sin^2\theta_1\sin^2\theta_2\sin 2\Phi$
5	$\lvert A_\parallel\rvert\lvert A_0\rvert$	$\cos(\delta_{2,1})$	$D\cos(\delta_{2,1})$	$C\cos\delta_{2,1}$	$-S\cos(\delta_{2,1})$	$\sqrt{2}\sin 2\theta_1\sin 2\theta_2\cos\Phi$
6	$\lvert A_0\rvert\lvert A_\perp\rvert$	$C\sin\delta_2$	$S\cos\delta_2$	$\sin\delta_2$	$D\cos\delta_2$	$-\sqrt{2}\sin 2\theta_1\sin 2\theta_2\sin\Phi$
7	$\lvert A_{SS}\rvert^2$	1	D	C	$-S$	$\frac{4}{9}$
8	$\lvert A_S\rvert^2$	1	$-D$	C	S	$\frac{4}{3}(\cos\theta_1+\cos\theta_2)^2$
9	$\lvert A_S\rvert\lvert A_{SS}\rvert$	$C\cos(\delta_S-\delta_{SS})$	$S\sin(\delta_S-\delta_{SS})$	$\cos(\delta_{SS}-\delta_S)$	$D\sin(\delta_{SS}-\delta_S)$	$\frac{8}{3\sqrt{3}}(\cos\theta_1+\cos\theta_2)$
10	$\lvert A_0\rvert\lvert A_{SS}\rvert$	$\cos\delta_{SS}$	$D\cos\delta_{SS}$	$C\cos\delta_{SS}$	$-S\cos\delta_{SS}$	$\frac{8}{3}\cos\theta_1\cos\theta_2$
11	$\lvert A_\parallel\rvert\lvert A_{SS}\rvert$	$\cos(\delta_{2,1}-\delta_{SS})$	$D\cos(\delta_{2,1}-\delta_{SS})$	$C\cos(\delta_{2,1}-\delta_{SS})$	$-S\cos(\delta_{2,1}-\delta_{SS})$	$\frac{4\sqrt{2}}{3}\sin\theta_1\sin\theta_2\cos\Phi$
12	$\lvert A_\perp\rvert\lvert A_{SS}\rvert$	$C\sin(\delta_2-\delta_{SS})$	$S\cos(\delta_2-\delta_{SS})$	$\sin(\delta_2-\delta_{SS})$	$D\cos(\delta_2-\delta_{SS})$	$-\frac{4\sqrt{2}}{3}\sin\theta_1\sin\theta_2\sin\Phi$
13	$\lvert A_0\rvert\lvert A_S\rvert$	$C\cos\delta_S$	$-S\sin\delta_S$	$\cos\delta_S$	$-D\sin\delta_S$	$\frac{8}{\sqrt{3}}\cos\theta_1\cos\theta_2\times(\cos\theta_1+\cos\theta_2)$
14	$\lvert A_\parallel\rvert\lvert A_S\rvert$	$C\cos(\delta_{2,1}-\delta_S)$	$S\sin(\delta_{2,1}-\delta_S)$	$\cos(\delta_{2,1}-\delta_S)$	$D\sin(\delta_{2,1}-\delta_S)$	$\frac{4\sqrt{2}}{\sqrt{3}}\sin\theta_1\sin\theta_2\times(\cos\theta_1+\cos\theta_2)\cos\Phi$
15	$\lvert A_\perp\rvert\lvert A_S\rvert$	$\sin(\delta_2-\delta_S)$	$-D\sin(\delta_2-\delta_S)$	$C\sin(\delta_2-\delta_S)$	$S\sin(\delta_2-\delta_S)$	$-\frac{4\sqrt{2}}{\sqrt{3}}\sin\theta_1\sin\theta_2\times(\cos\theta_1+\cos\theta_2)\sin\Phi$

where ϕ_s measures CP violation in the interference between the direct decay amplitude and that via mixing, $\lambda \equiv (q/p)(\bar{A}/A)$, q and p are the complex parameters relating the B_s^0 flavor and mass eigenstates, and $A(\bar{A})$ is the decay amplitude (CP conjugate decay amplitude). Under the assumption that $|q/p| = 1$, $|\lambda|$ measures direct CP violation. The CP violation parameters are assumed to be helicity independent. The association of ϕ_s and $|\lambda|$ with S-wave and double S-wave terms implies that these consist solely of contributions with the same flavor content as the ϕ meson, i.e. an $s\bar{s}$ resonance.

In Table I, δ_S and δ_{SS} are the strong phases of the $P \to VS$ and $P \to SS$ processes, respectively. The P-wave strong phases are defined to be $\delta_1 \equiv \delta_\perp - \delta_\parallel$ and $\delta_2 \equiv \delta_\perp - \delta_0$, with the notation $\delta_{2,1} \equiv \delta_2 - \delta_1$.

B. Triple-product asymmetries

Scalar triple products of three momentum or spin vectors are odd under time reversal, T. Nonzero asymmetries for these observables can either be due to a CP-violating phase or a CP-conserving phase and final-state interactions. Four-body final states give rise to three independent momentum vectors in the rest frame of the decaying B_s^0 meson. For a detailed review of the phenomenology the reader is referred to Ref. [9].

The two independent terms in the time-dependent decay rate that contribute to a T-odd asymmetry are the $K_4(t)$ and $K_6(t)$ terms, defined in Eq. (3). The triple products that allow access to these terms are

$$\sin\Phi = (\hat{n}_{V_1} \times \hat{n}_{V_2}) \cdot \hat{p}_{V_1}, \tag{7}$$

$$\sin 2\Phi = 2(\hat{n}_{V_1} \cdot \hat{n}_{V_2})(\hat{n}_{V_1} \times \hat{n}_{V_2}) \cdot \hat{p}_{V_1}, \tag{8}$$

where $\hat{n}_{V_i}$ $(i = 1, 2)$ is a unit vector perpendicular to the V_i decay plane and $\hat{p}_{V_1}$ is a unit vector in the direction of V_1 in the B_s^0 rest frame, defined in Fig. 2. This then provides a method of probing CP violation without the need to measure the decay time or the initial flavor of the B_s^0 meson. It should be noted that, while the observation of nonzero triple-product asymmetries implies CP violation or final-state interactions (in the case of B_s^0 meson decays), the measurements of triple-product asymmetries consistent with zero do not rule out the presence of CP-violating effects, as strong phase differences can cause suppression [9].

In the $B_s^0 \to \phi\phi$ decay, two triple products are defined as $U \equiv \sin\Phi\cos\Phi$ and $V \equiv \sin(\pm\Phi)$ where the positive sign is taken if $\cos\theta_1 \cos\theta_2 \geq 0$ and negative sign otherwise.

The T-odd asymmetry corresponding to the U observable, A_U, is defined as the normalized difference between the number of decays with positive and negative values of $\sin\Phi\cos\Phi$,

$$A_U \equiv \frac{\Gamma(U > 0) - \Gamma(U < 0)}{\Gamma(U > 0) + \Gamma(U < 0)} \propto \int_0^\infty \Im(A_\perp(t)A_\parallel^*(t) + \bar{A}_\perp(t)\bar{A}_\parallel^*(t))\mathrm{d}t. \tag{9}$$

Similarly A_V is defined as

$$A_V \equiv \frac{\Gamma(V > 0) - \Gamma(V < 0)}{\Gamma(V > 0) + \Gamma(V < 0)} \propto \int_0^\infty \Im(A_\perp(t)A_0^*(t) + \bar{A}_\perp(t)\bar{A}_0^*(t))\mathrm{d}t. \tag{10}$$

Extraction of the triple-product asymmetries is then reduced to a simple counting exercise.

V. DECAY TIME RESOLUTION

The sensitivity to ϕ_s is affected by the accuracy of the measured decay time. To resolve the fast B_s^0-$\bar{B}_s^0$ oscillation period of approximately 355 fs, it is necessary to have a decay time resolution that is much smaller than this. To account for decay time resolution, all decay time-dependent terms are convolved with a Gaussian function, with width σ_i^t that is estimated for each event, i, based upon the uncertainty obtained from the vertex and kinematic fit. To apply an event-dependent resolution model during fitting, the estimated per-event decay time uncertainty must be calibrated. This is done using simulated events that are divided into bins of σ_i^t. For each bin, a Gaussian function is fitted to the difference between reconstructed decay time and the true decay time to determine the resolution σ_{true}^t. A first-order polynomial is then fitted to the distribution of σ_i^t vs σ_{true}^t, with parameters denoted by q_0 and q_1. The calibrated per-event decay time uncertainty used in the decay time-dependent fit is then calculated as $\sigma_i^{\text{cal}} = q_0 + q_1\sigma_i^t$. Gaussian constraints are used to account for the uncertainties on the calibration parameters in the decay time-dependent fit. Cross-checks, consisting of the variation of an effective single Gaussian resolution far beyond the observed differences in data and simulated events yield negligible modifications to results; hence, no systematic uncertainty is assigned. The results are verified to be largely insensitive to the details of the resolution model, as supported by tests on data and observed in similar measurements [6].

The effective single Gaussian resolution is found from simulated data sets to be 41.4 ± 0.5 and 43.9 ± 0.5 fs for the 2011 and 2012 data sets, respectively. Differences in the resolutions from 2011 and 2012 data sets are expected due to the independent selection requirements.

VI. ACCEPTANCES

The four observables used to analyze $B_s^0 \to \phi\phi$ events consist of the decay time and the three helicity angles,

which require a good understanding of efficiencies in these variables. It is assumed that the decay time and angular acceptances factorize.

A. Angular acceptance

The geometry of the LHCb detector and the momentum requirements imposed on the final-state particles introduce efficiencies that vary as functions of the helicity angles. Simulated events with the same selection criteria as those applied to $B_s^0 \to \phi\phi$ data events are used to determine this efficiency correction. Efficiencies as a function of the three helicity angles are shown in Fig. 3.

Acceptance functions are included in the decay time-dependent fit through the 15 integrals $\int \epsilon(\Omega) f_k(\Omega) \mathrm{d}\Omega$, where f_k are the angular functions given in Table I and $\epsilon(\Omega)$ is the efficiency as a function of the set of helicity angles, Ω. The inclusion of the integrals in the normalization of the probability density function (PDF) is sufficient to describe the angular acceptance as the acceptance factors for each event appear as a constant in the log likelihood, the construction of which is described in detail in Sec. VIII A, and therefore do not affect the fitted parameters. The method for the calculation of the integrals is described in detail in Ref. [36]. The integrals are calculated correcting for the differences between data and simulated events. This includes differences in the BDT training variables that can affect acceptance corrections through correlations with the helicity angles.

The fit to determine the triple-product asymmetries assumes that the U and V observables are symmetric in the acceptance corrections. Simulated events are then used to assign a systematic uncertainty related to this assumption.

B. Decay time acceptance

The impact parameter requirements on the final-state particles efficiently suppress the background from numerous pions and kaons originating from the PV but introduce a decay time dependence in the selection efficiency.

The efficiency as a function of the decay time is taken from $B_s^0 \to D_s^-(\to K^+K^-\pi^-)\pi^+$ data events, with an upper limit of 1 ps applied to the D_s^- decay time to ensure topological similarity to the $B_s^0 \to \phi\phi$ decay. After the same decay time-biasing selections are applied to the $B_s^0 \to D_s^-\pi^+$ decay as used in the $B_s^0 \to \phi\phi$ decay, $B_s^0 \to D_s^-\pi^+$ events are reweighted according to the minimum track transverse momentum to ensure the closest agreement between the time acceptances of $B_s^0 \to \phi\phi$ and $B_s^0 \to D_s^-\pi^+$ simulated events. The denominator used to calculate the decay time acceptance in $B_s^0 \to D_s^-\pi^+$ data is taken from a simulated data set, generated with the B_s^0 lifetime taken from the value measured by the LHCb experiment [37].

For the case of the decay time-dependent fit, the efficiency as a function of the decay time is modelled as a histogram, with systematic uncertainties arising from the differences in $B_s^0 \to \phi\phi$ and $B_s^0 \to D_s^-\pi^+$ simulated events. Figure 4 shows the comparison of the efficiency as a function of decay time calculated using $B_s^0 \to D_s^-\pi^+$ data in 2011 and 2012. Also shown is the comparison between $B_s^0 \to \phi\phi$ and $B_s^0 \to D_s^-\pi^+$ simulated events.

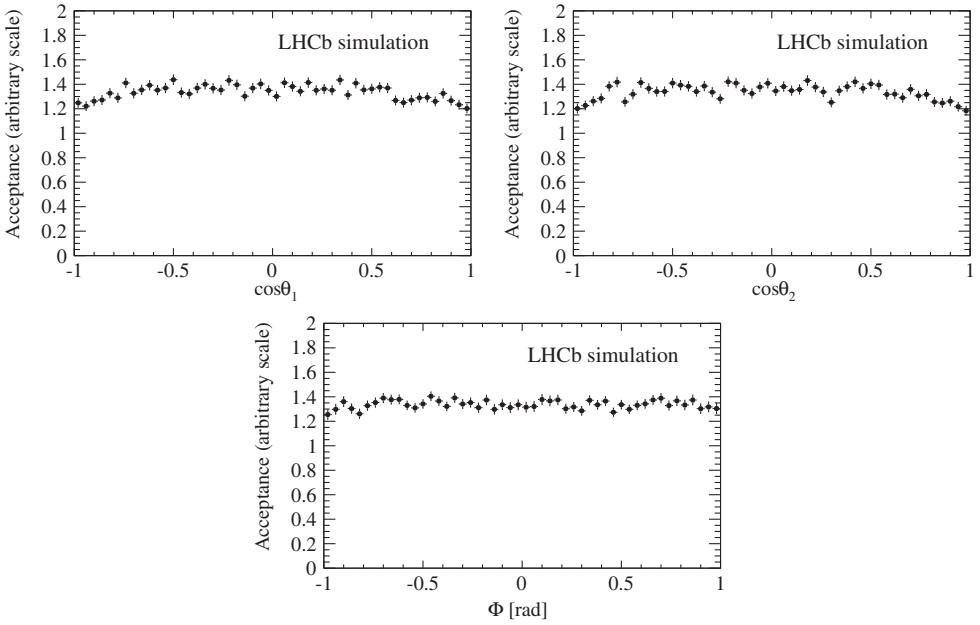

FIG. 3. Angular acceptance found from simulated $B_s^0 \to \phi\phi$ events (top-left) integrated over $\cos\theta_2$ and Φ as a function of $\cos\theta_1$, (top-right) integrated over $\cos\theta_1$ and Φ as a function of $\cos\theta_2$, and (bottom) integrated over $\cos\theta_1$ and $\cos\theta_2$ as a function of Φ.

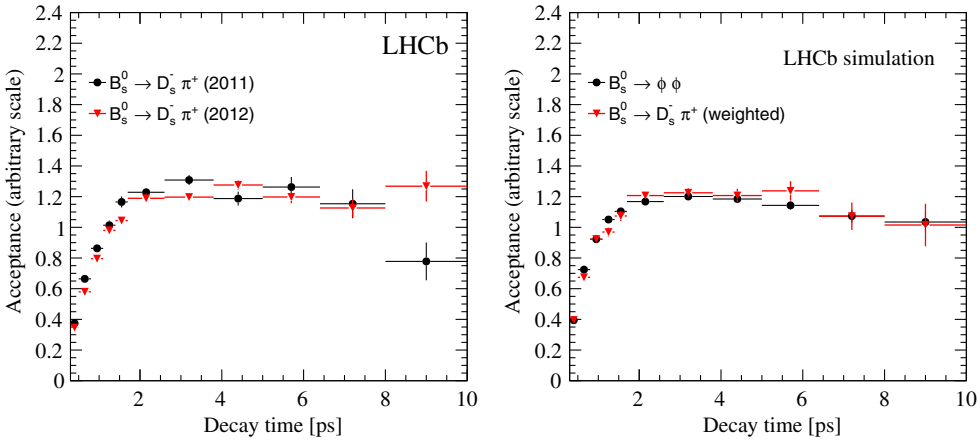

FIG. 4 (color online). Decay time acceptance (left) calculated using $B_s^0 \to D_s^- \pi^+$ data events and (right) comparing $B_s^0 \to \phi\phi$ and $B_s^0 \to D_s^- \pi^+$ simulation, where $B_s^0 \to D_s^- \pi^+$ events are reweighted to match the distribution of the minimum p_T of the final-state particles in $B_s^0 \to \phi\phi$ decays.

In the fit to determine the triple-product asymmetries, the decay time acceptance is treated only as a systematic uncertainty, which is based on the acceptance found from $B_s^0 \to D_s^- \pi^+$ data events.

VII. FLAVOR TAGGING

To maximize the sensitivity on ϕ_s, the determination of the initial flavor of the B_s^0 meson is necessary. This results from the terms in the differential decay rate with the largest sensitivity to ϕ_s requiring the identification (tagging) of the flavor at production. At the LHCb, tagging is achieved through the use of different algorithms described in Refs. [6,38]. This analysis uses both the opposite side (OS) and same side kaon (SSK) flavor taggers.

The OS flavor tagging algorithm [39] makes use of the $\bar{b}(b)$-quark produced in association with the signal $b(\bar{b})$ quark. In this analysis, the predicted probability of an incorrect flavor assignment, ω, is determined for each event by a neural network that is calibrated using $B^+ \to J/\psi K^+$, $B^+ \to \bar{D}^0 \pi^+$, $B^0 \to J/\psi K^{*0}$, $B^0 \to D^{*-} \mu^+ \nu_\mu$, and $B_s^0 \to D_s^- \pi^+$ data as control modes. Details of the calibration procedure can be found in Ref. [6].

When a signal B_s^0 meson is formed, there is an associated $\bar{s}$ quark formed in the first branches of the fragmentation that about 50% of the time forms a charged kaon, which is likely to originate close to the B_s^0 meson production point. The kaon charge therefore allows for the identification of the flavor of the signal B_s^0 meson. This principle is exploited by the SSK flavor tagging algorithm [38]. The SSK tagger is calibrated with the $B_s^0 \to D_s^+ \pi^-$ decay mode. A neural network is used to select fragmentation particles, improving the flavor tagging power quoted in the previous decay time-dependent measurement [17,40].

Flavor tagging power is defined as $\epsilon_{\rm tag} \mathcal{D}^2$, where $\epsilon_{\rm tag}$ is the flavor tagging efficiency and $\mathcal{D} \equiv (1 - 2\omega)$ is the dilution. Table II shows the tagging power for the events tagged by only one of the algorithms and those tagged by both, estimated from 2011 and 2012 $B_s^0 \to \phi\phi$ data events separately. Uncertainties due to the calibration of the flavor tagging algorithms are applied as Gaussian constraints in the decay time-dependent fit. The dependence of the flavor tagging initial flavor of the B_s^0 meson is accounted for during fitting.

VIII. DECAY TIME-DEPENDENT MEASUREMENT

A. Likelihood

The parameters of interest are the *CP*-violation parameters (ϕ_s and $|\lambda|$), the polarization amplitudes ($|A_0|^2$, $|A_\perp|^2$, $|A_S|^2$, and $|A_{SS}|^2$), and the strong phases (δ_1, δ_2, δ_S, and δ_{SS}), as defined in Sec. IV A. The *P*-wave amplitudes are defined such that $|A_0|^2 + |A_\perp|^2 + |A_\parallel|^2 = 1$; hence, only two are free parameters.

Parameter estimation is achieved from a minimization of the negative log likelihood. The likelihood, $\mathcal{L}$, is weighted using the *sPlot* method [41,42], with the signal weight of an event e calculated from the equation

TABLE II. Tagging efficiency ($\epsilon_{\rm tag}$), effective dilution ($\mathcal{D}$), and tagging power ($\epsilon\mathcal{D}^2$), as estimated from the data for events tagged containing information from OS algorithms only, SSK algorithms only, and information from both algorithms. Quoted uncertainties include both statistical and systematic contributions.

Data set	$\epsilon_{\rm tag}(\%)$	$\mathcal{D}(\%)$	$\epsilon\mathcal{D}^2(\%)$
2011 OS	12.3 ± 1.0	31.6 ± 0.2	1.23 ± 0.10
2012 OS	14.5 ± 0.7	32.7 ± 0.3	1.55 ± 0.08
2011 SSK	40.2 ± 1.4	15.2 ± 2.0	0.93 ± 0.25
2012 SSK	33.1 ± 0.9	16.0 ± 1.6	0.85 ± 0.17
2011 both	26.0 ± 1.3	34.9 ± 1.1	3.17 ± 0.26
2012 both	27.5 ± 0.9	33.2 ± 1.2	3.04 ± 0.24

$$W_e(m_{K^+K^-K^+K^-}) = \frac{\sum_j V_{sj} F_j(m_{K^+K^-K^+K^-})}{\sum_j N_j F_j(m_{K^+K^-K^+K^-})}, \quad (11)$$

where j sums over the number of fit components to the four-kaon invariant mass, with PDFs F, associated yields N, and V_{sj} is the covariance between the signal yield and the yield associated with the jth fit component. The log likelihood then takes the form

$$-\ln\mathcal{L} = -\alpha \sum_{\text{events } e} W_e \ln(S^e_{\text{TD}}), \quad (12)$$

where $\alpha = \sum_e W_e / \sum_e W_e^2$ is used to account for the weights in the determination of the statistical uncertainties, and S_{TD} is the signal model of Eq. (2), accounting also for the effects of decay time and angular acceptance, in addition to the probability of an incorrect flavor tag. Explicitly, this can be written as

$$S^e_{\text{TD}} = \frac{\sum_i s^e_i(t_e) f_i(\Omega_e)\epsilon(t_e)}{\sum_k \zeta_k \int s_k(t) f_k(\Omega)\epsilon(t)\mathrm{d}t\mathrm{d}\Omega}, \quad (13)$$

where ζ_k are the normalization integrals used to describe the angular acceptance described in Sec. VI A and

$$s^e_i(t) = N_i e^{-\Gamma_s t_e}\Big[c_i q_e(1-2\omega_e)\cos(\Delta m_s t_e) + d_i q_e(1-2\omega_e)\sin(\Delta m_s t_e) + a_i \cosh\left(\frac{1}{2}\Delta\Gamma_s t_e\right) + b_i \sinh\left(\frac{1}{2}\Delta\Gamma_s t_e\right)\Big] \otimes R(\sigma^{\text{cal}}_e, t_e), \quad (14)$$

where ω_e is the calibrated probability of an incorrect flavor assignment and R denotes the Gaussian resolution function. In Eq. (14), $q_e = 1(-1)$ for a B^0_s ($\bar{B}^0_s$) meson at $t = 0$ in event e or $q_e = 0$ if no flavor tagging information exists. The 2011 and 2012 data samples are assigned independent signal weights, decay time and angular acceptances, in addition to separate Gaussian constraints to the decay time resolution parameters as defined in Sec. V. The value of the B^0_s-$\bar{B}^0_s$ oscillation frequency is constrained to the LHCb measured value of $\Delta m_s = 17.768 \pm 0.023(\text{stat}) \pm 0.006(\text{syst})\ \text{ps}^{-1}$ [43]. The values of the decay width and decay width difference are constrained to the LHCb measured values of $\Gamma_s = 0.661 \pm 0.004(\text{stat}) \pm 0.006(\text{syst})\ \text{ps}^{-1}$ and $\Delta\Gamma_s = 0.106 \pm 0.011(\text{stat}) \pm 0.007(\text{syst})\ \text{ps}^{-1}$, respectively [6]. The Gaussian constraints applied to the Γ_s and $\Delta\Gamma_s$ parameters use the combination of the measured values from $B^0_s \to J/\psi K^+K^-$ and $B^0_s \to J/\psi\pi^+\pi^-$ decays. Constraints are therefore applied taking into account a correlation of 0.1 for the statistical uncertainties [6]. The systematic uncertainties are taken to be uncorrelated between the $B^0_s \to J/\psi K^+K^-$ and $B^0_s \to J/\psi\pi^+\pi^-$ decay modes.

The events selected in this analysis are within the two-kaon invariant mass range $994.5 < m_{K^+K^-} < 1044.5\ \text{MeV}/c^2$ and are divided into three regions. These correspond to both ϕ candidates with invariant masses smaller than the known ϕ mass, one ϕ candidate with an invariant mass smaller than the known ϕ mass and one larger, and a third region in which both ϕ candidates have invariant masses larger than the known ϕ mass. Binning the data in this way allows the analysis to become insensitive to correction factors that must be applied to each of the S-wave and double S-wave interference terms in the differential cross section. These factors modulate the contributions of the interference terms in the angular PDF due to the different line shapes of kaon pairs originating from spin-1 and spin-0 configurations. Their parametrizations are denoted by $g(m_{K^+K^-})$ and $h(m_{K^+K^-})$, respectively. The spin-1 configuration is described by a Breit–Wigner function, and the spin-0 configuration is assumed to be approximately uniform. The correction factors, denoted by C_{SP}, are defined from the relation [6]

$$C_{SP} e^{i\theta_{SP}} = \int_{m_{\text{l}}}^{m_{\text{h}}} g^*(m_{K^+K^-}) h(m_{K^+K^-}) \mathrm{d}m_{K^+K^-}, \quad (15)$$

where m_{h} and m_{l} are the upper and lower edges of a given $m_{K^+K^-}$ bin, respectively. Alternative assumptions on the P-wave and S-wave line shapes are found to have a negligible effect on the parameter estimation.

A simultaneous fit is then performed in the three $m_{K^+K^-}$ invariant mass regions, with all parameters shared except for the fractions and strong phases associated with the S wave and double S wave, which are allowed to vary independently in each region. The correction factors are calculated as described in Ref. [6]. The correction factor used for each region is calculated to be 0.69.

B. RESULTS

The results of the fit to the parameters of interest are given in Table III. The S-wave and double S-wave parameter estimations for the three regions defined in Sec. VIII A are given in Table IV. The fraction of the S

TABLE III. Results of the decay time-dependent fit.

Parameter	Best fit value
ϕ_s (rad)	-0.17 ± 0.15
$\lvert\lambda\rvert$	1.04 ± 0.07
$\lvert A_\perp\rvert^2$	0.305 ± 0.013
$\lvert A_0\rvert^2$	0.364 ± 0.012
δ_1 (rad)	0.13 ± 0.23
δ_2 (rad)	2.67 ± 0.23
Γ_s (ps^{-1})	0.662 ± 0.006
$\Delta\Gamma_s$ (ps^{-1})	0.102 ± 0.012
Δm_s (ps^{-1})	17.774 ± 0.024

TABLE IV. *S*-wave and double *S*-wave results of the decay time-dependent fit for the three regions identified in Sec. VIII A, where M_{--} indicates the region with both two-kaon invariant masses smaller than the known ϕ mass, M_{-+} indicates the region with one smaller and one larger, and M_{++} indicates the region with both two-kaon invariant masses larger than the known ϕ mass.

Region	$\lvert A_S\rvert^2$	δ_S (rad)	$\lvert A_{SS}\rvert^2$	δ_{SS} (rad)
M_{--}	0.006 ± 0.012	-0.40 ± 0.53	0.009 ± 0.016	-2.99 ± 1.27
M_{-+}	0.006 ± 0.010	2.76 ± 0.39	0.004 ± 0.011	-2.17 ± 0.72
M_{++}	0.001 ± 0.003	-2.58 ± 2.08	0.020 ± 0.022	0.53 ± 0.55

TABLE V. Correlation matrix associated with the result of the decay time-dependent fit. Correlations with a magnitude greater than 0.5 are shown in bold.

	$\lvert A_\perp\rvert^2$	$\lvert A_0\rvert^2$	$\lvert A_{SS}\rvert^2$	$\lvert A_S\rvert^2$	δ_{SS}	δ_S	δ_1	δ_2	ϕ_s	$\lvert\lambda\rvert$
$\lvert A_\perp\rvert^2$	1.00	−0.48	0.01	0.07	0.00	0.01	−0.04	0.01	−0.13	−0.01
$\lvert A_0\rvert^2$		1.00	−0.02	−0.14	−0.03	0.01	0.05	0.02	0.07	0.03
$\lvert A_{SS}\rvert^2$			1.00	0.18	**0.59**	0.01	0.04	0.07	−0.03	−0.18
$\lvert A_S\rvert^2$				1.00	0.21	0.01	0.01	0.06	−0.03	−0.25
δ_{SS}					1.00	−0.02	0.03	0.06	−0.06	−0.21
δ_S						1.00	0.40	0.42	−0.07	−0.16
δ_1							1.00	**0.95**	−0.20	−0.27
δ_2								1.00	−0.20	−0.28
ϕ_s									1.00	0.12
$\lvert\lambda\rvert$										1.00

wave is found to be consistent with zero in all three mass regions.

The correlation matrix is shown in Table V. The largest correlations are found to be between the amplitudes themselves and the *CP*-conserving strong phases themselves. The observed correlations have been verified with simulated data sets. Cross-checks are performed on simulated data sets generated with the same number of events as observed in data, and with the same physics parameters, to ensure that generation values are recovered with negligible biases.

Figure 5 shows the distributions of the B_s^0 decay time and the three helicity angles. Superimposed are the projections of the fit result. The projections are event weighted to yield the signal distribution and include acceptance effects.

The scan of the natural logarithm of the likelihood for the ϕ_s parameter is shown in Fig. 6. At each point in the scan, all other parameters are reminimized. A parabolic minimum is observed and a point estimate provided. The shape of the profile log likelihood is replicated in simplified simulations as a cross-check.

C. Systematic uncertainties

The most significant systematic effects arise from the angular and decay time acceptances. Minor contributions are also found from the mass model used to construct the event weights, the uncertainty on the peaking background contributions, and the fit bias.

An uncertainty due to the angular acceptance arises from the limited number of simulated events used to determine the acceptance correction. This is accounted for by varying the normalization weights within their statistical uncertainties accounting for correlations. The varied weights are then used to fit simulated data sets. This process is repeated, and the width of the Gaussian distribution is used as the uncertainty. A further uncertainty arises from the assumption that the angular acceptance does not depend on the algorithm used for the initial flavor assignment. Such a dependence can be expected due to the kinematic correlations of the tagging particles with the signal particles. This introduces a tagging efficiency based on the kinematics of the signal particles. The difference between the nominal data result and the result with angular acceptances calculated independently for the different flavor tagging algorithms leads to a non-negligible uncertainty on the polarization amplitudes. Further checks are performed to verify that the angular acceptance does not depend on the way in which the event was triggered.

The systematic uncertainty on the decay time acceptance is evaluated from the difference in the decay time acceptance evaluated from $B_s^0 \to \phi\phi$ and $B_s^0 \to D_s^- \pi^+$ simulated events. The simulated data sets are generated with the decay time acceptance of $B_s^0 \to \phi\phi$ simulation and then fitted with the $B_s^0 \to D_s^- \pi^+$ decay time acceptance. This process is repeated, and the resulting bias on the fitted parameters is used as an estimate of the systematic uncertainty.

The uncertainty on the mass model is found by refitting the data with signal weights derived from a single Gaussian $B_s^0 \to \phi\phi$ model, rather than the nominal double Gaussian. The uncertainty due to peaking background contributions is found through the recalculation of the signal weights with

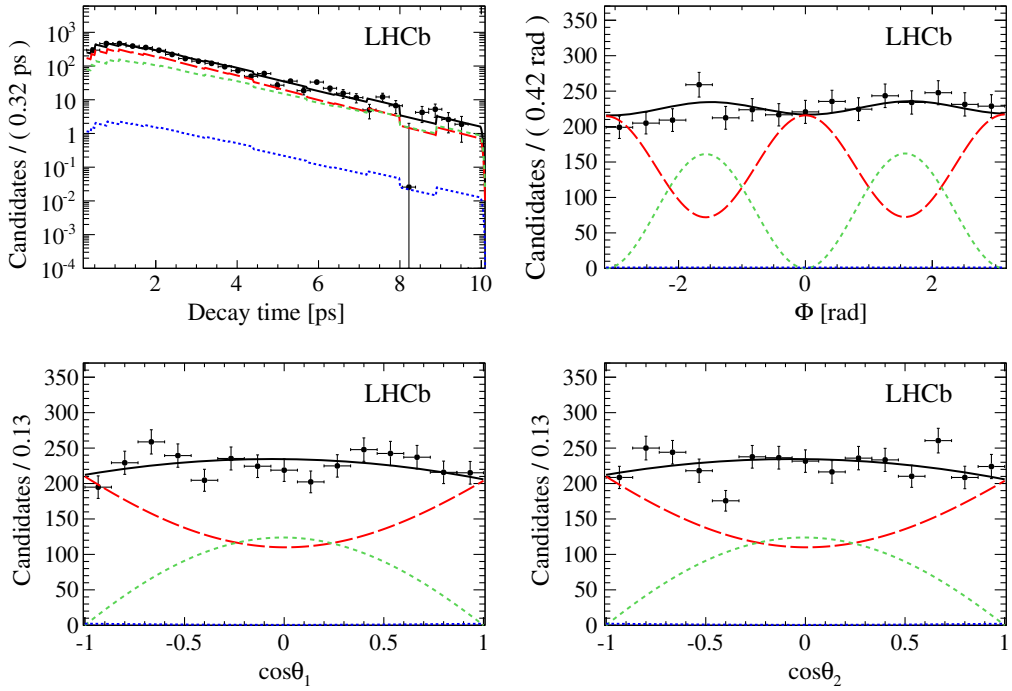

FIG. 5 (color online). One-dimensional projections of the $B_s^0 \to \phi\phi$ fit for (top-left) decay time with binned acceptance, (top-right) helicity angle Φ, and (bottom-left and bottom-right) cosine of the helicity angles θ_1 and θ_2. The background-subtracted data are marked as black points, while the black solid lines represent the projections of the best fit. The CP-even P-wave, the CP-odd P-wave, and S-wave combined with double S-wave components are shown by the red long-dashed, green short-dashed, and blue dotted lines, respectively.

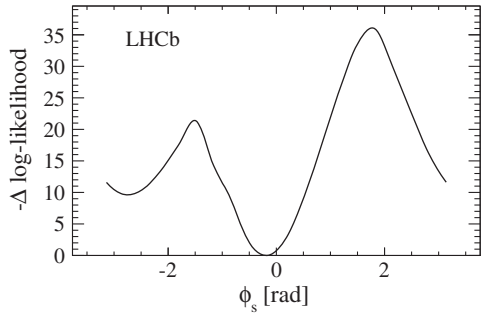

FIG. 6. Profile log likelihood for the ϕ_s parameter.

peaking background contributions varied according to the statistical uncertainties on the yields of the $\Lambda_b^0 \to \phi p K^-$ and $B^0 \to \phi K^{*0}$ contributions. Fit bias arises in likelihood fits when the number of events used to determine the free parameters is not sufficient to achieve the Gaussian limit. This uncertainty is evaluated by generating and fitting simulated data sets and taking the resulting bias as the uncertainty.

Uncertainties due to flavor tagging are included in the statistical uncertainty through Gaussian constraints on the calibration parameters and amount to 10% of the statistical uncertainty on the CP-violating phase.

A summary of the systematic uncertainties is given in Table VI.

IX. TRIPLE-PRODUCT ASYMMETRIES

A. Likelihood

To determine the triple-product asymmetries, a separate likelihood fit is performed. This is based around the simultaneous fitting of separate data sets to the four-kaon invariant mass, which are split according to the sign of U and V observables. Simultaneous mass fits are performed for the U and V observables separately. The set of free parameters in fits to determine the U and V observables consist of the asymmetries of the $B_s^0 \to \phi\phi$ signal and combinatoric background ($A_{U(V)}$ and $A^{\mathrm{B}}_{U(V)}$), along with their associated total yields (N_{S} and N_{B}). The mass model is the same as that described in Sec. III. The total PDF, S_{TP}, is then of the form

$$S_{\mathrm{TP}} = \sum_{i\in\{+,-\}} \left(f_i^S G^S(m_{K^+K^-K^+K^-}) + \sum_j f_i^j P^j(m_{K^+K^-K^+K^-}) \right), \tag{16}$$

where j indicates the sum over the background components with corresponding PDFs, P^j, and G^S is the double Gaussian signal PDF as described in Sec. III. The parameters f_i^k found in Eq. (16) are related to the asymmetry, $A^k_{U(V)}$, through

TABLE VI. Summary of systematic uncertainties for physics parameters in the decay time-dependent measurement, where AA denotes angular acceptance.

Parameter	$\lvert A_0\rvert^2$	$\lvert A_\perp\rvert^2$	δ_1 (rad)	δ_2 (rad)	ϕ_s (rad)	$\lvert\lambda\rvert$
Mass model	–	–	0.03	0.04	–	0.02
AA (statistical)	0.003	0.004	0.02	0.02	0.02	0.02
AA (tagging)	0.006	0.002	–	0.01	–	0.01
Fit bias	–	–	0.02	–	–	–
Time acceptance	0.005	0.003	0.02	0.05	0.02	–
Peaking background	–	–	0.01	0.01	–	0.01
Total	0.009	0.005	0.05	0.07	0.03	0.03

$$f_+^k = \frac{1}{2}(A_{U(V)}^k + 1), \tag{17}$$

$$f_-^k = \frac{1}{2}(1 - A_{U(V)}^k), \tag{18}$$

where k denotes a four-kaon mass fit component, as described in Sec. III. Peaking backgrounds are assumed to be symmetric in U and V.

B. Results

The background-subtracted distributions of the U and V observables are shown in Fig. 7 for the mass range $5246.8 < m_{K^+K^-K^+K^-} < 5486.8$ MeV$/c^2$. Distributions are found to agree between 2011 and 2012 data sets and show qualitatively symmetric distributions. The triple-product asymmetries found from the simultaneous fit described in Sec. IX A are measured to be

$$A_U = -0.003 \pm 0.017,$$
$$A_V = -0.017 \pm 0.017.$$

Statistical uncertainties are therefore to have approximately halved with respect to the previous LHCb measurements [19], due to more efficient selection requirements and a larger data sample, and are verified through fits to simulated data sets. No evidence for *CP* violation is found.

C. Systematic uncertainties

As for the case of the decay time-dependent fit, the largest contributions to the systematic uncertainty arise from the decay time and angular acceptances. Minor uncertainties also result from the mass model and peaking background knowledge.

The effect of the decay time acceptance is determined through the generation of simulated samples including the decay time acceptance obtained from $B_s^0 \to D_s^-\pi^+$ data and fitted with the method described in Sec. IX A. The resulting bias is used to assign a systematic uncertainty.

The effect of the angular acceptance is evaluated by generating simulated data sets with and without the inclusion of the angular acceptance. The resulting bias found on the fit results of the triple-product asymmetries is then used as a systematic uncertainty.

Uncertainties related to the mass model are evaluated by taking the difference between the nominal fit results and

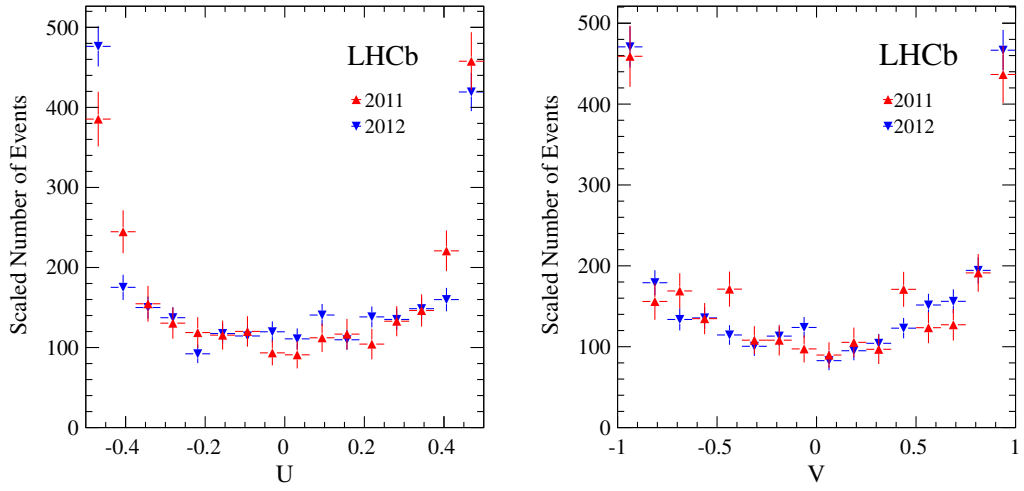

FIG. 7 (color online). Background-subtracted distributions of the (left) U and (right) V observables for the 2011 and 2012 data sets and restricted to the mass range $5246.8 < m_{K^+K^-K^+K^-} < 5486.8$ MeV$/c^2$. The 2011 distributions are scaled to have the same area as the 2012 distributions.

TABLE VII. Systematic uncertainties on the triple-product asymmetries A_U and A_V. The total uncertainty is the sum in quadrature of the larger of the two components for each source.

Source	A_U	A_V	Uncertainty
Angular acceptance	0.001	0.003	0.003
Time acceptance	0.005	0.003	0.005
Mass model	0.002	0.002	0.002
Peaking background	–	0.001	0.001
Total	0.006	0.005	0.006

those using a single Gaussian function to model the $B_s^0 \to \phi\phi$ decay. The effect of the peaking background is evaluated by taking the largest difference between the nominal fit results and the fit results with the peaking background yields varied according to their uncertainties, as given in Sec. III.

The total systematic uncertainty is estimated by choosing the larger of the two individual systematic uncertainties on A_U and A_V. The contributions are combined in quadrature to determine the total systematic uncertainty.

Systematic uncertainties due to the residual effect of the decay time, geometrical acceptance, and the signal and background fit models are summarized in Table VII.

X. SUMMARY AND CONCLUSIONS

Measurements of CP violation in the $B_s^0 \to \phi\phi$ decay are presented, based on the full LHCb run 1 data set of 3.0 fb^{-1}. The CP-violating phase, ϕ_s, and CP-violation parameter, $|\lambda|$, are determined to be

$$\phi_s = -0.17 \pm 0.15(\text{stat}) \pm 0.03(\text{stat}) \text{ rad},$$
$$|\lambda| = 1.04 \pm 0.07(\text{stat}) \pm 0.03(\text{syst}).$$

Results are found to agree with the theoretical predictions [1–3]. When compared with the CP-violating phase measured in $B_s^0 \to J/\psi K^+K^-$ and $B_s^0 \to J/\psi\pi^+\pi^-$ decays [6], these results show that no large CP violation is present either in B_s^0-$\bar{B}_s^0$ mixing or in the $\bar{b} \to \bar{s}s\bar{s}$ decay amplitude.

The polarization amplitudes and strong phases are measured to be

$$|A_0|^2 = 0.364 \pm 0.012(\text{stat}) \pm 0.009(\text{syst}),$$
$$|A_\perp|^2 = 0.305 \pm 0.013(\text{stat}) \pm 0.005(\text{syst}),$$
$$\delta_1 = 0.13 \pm 0.23(\text{stat}) \pm 0.05(\text{syst}) \text{ rad},$$
$$\delta_2 = 2.67 \pm 0.23(\text{stat}) \pm 0.07(\text{syst}) \text{ rad}.$$

Values of the polarization amplitudes are found to agree well with the previous measurements [17–19]. Measurements in other $B \to VV$ penguin transitions at the B factories generally give higher values of $f_L \equiv |A_0|^2$ [11–16]. The value of f_L found in the $B_s^0 \to \phi\phi$ channel is almost equal to that in the $B_s^0 \to K^{*0}\bar{K}^{*0}$ decay [44]. As reported in Ref. [19], the results are in agreement with QCD factorization predictions [2,3] but disfavor the perturbative QCD estimate given in Ref. [45]. The fractions of S wave and double S wave are found to be consistent with zero in all three regions of $m_{K^+K^-}$ mass.

The triple-product asymmetries are determined from a separate decay time integrated fit to be

$$A_U = -0.003 \pm 0.017(\text{stat}) \pm 0.006(\text{syst}),$$
$$A_V = -0.017 \pm 0.017(\text{stat}) \pm 0.006(\text{syst}),$$

in agreement with previous measurements [18,19].

The results of the polarization amplitudes, strong phases, and triple-product asymmetries presented in this paper supersede the previous LHCb measurements [17,19]. The measured values of the CP-violating phase and triple-product asymmetries are consistent with the hypothesis of CP conservation.

ACKNOWLEDGMENTS

We express our gratitude to our colleagues in the CERN accelerator departments for the excellent performance of the LHC. We thank the technical and administrative staff at the LHCb institutes. We acknowledge support from CERN and from the national agencies: CAPES, CNPq, FAPERJ, and FINEP (Brazil); NSFC (China); CNRS/IN2P3 (France); BMBF, DFG, HGF, and MPG (Germany); SFI (Ireland); INFN (Italy); FOM and NWO (Netherlands); MNiSW and NCN (Poland); MEN/IFA (Romania); MinES and FANO (Russia); MinECo (Spain); SNSF and SER (Switzerland); NASU (Ukraine); STFC (United Kingdom); and NSF (USA). The Tier1 computing centers are supported by IN2P3 (France), KIT and BMBF (Germany), INFN (Italy), NWO and SURF (Netherlands), PIC (Spain), and GridPP (United Kingdom). We are indebted to the communities behind the multiple open source software packages on which we depend. We are also thankful for the computing resources and the access to software research and development tools provided by Yandex LLC (Russia). Individual groups or members have received support from EPLANET, Marie Skłodowska-Curie Actions and ERC (European Union), Conseil général de Haute-Savoie, Labex ENIGMASS and OCEVU, Région Auvergne (France), RFBR (Russia), XuntaGal and GENCAT (Spain), Royal Society and Royal Commission for the Exhibition of 1851 (United Kingdom).

[1] M. Bartsch, arXiv:0810.0249.
[2] M. Beneke, J. Rohrer, and D. Yang, Nucl. Phys. **B774**, 64 (2007).
[3] H.-Y. Cheng and C.-K. Chua, Phys. Rev. D **80**, 114026 (2009).
[4] M. Kobayashi and T. Maskawa, Prog. Theor. Phys. **49**, 652 (1973); N. Cabibbo, Phys. Rev. Lett. **10**, 531 (1963).
[5] J. Charles *et al.*, Phys. Rev. D **84**, 033005 (2011).
[6] R. Aaij *et al.* (LHCb Collaboration), Phys. Rev. D **87**, 112010 (2013).
[7] R. Aaij *et al.* (LHCb Collaboration), Phys. Lett. B **736**, 186 (2014).
[8] R. Aaij *et al.* (LHCb Collaboration), Eur. Phys. J. C **73**, 2373 (2013).
[9] M. Gronau and J. L. Rosner, Phys. Rev. D **84**, 096013 (2011).
[10] A. Datta, M. Duraisamy, and D. London, Phys. Rev. D **86**, 076011 (2012).
[11] K.-F. Chen *et al.* (Belle Collaboration), Phys. Rev. Lett. **94**, 221804 (2005).
[12] B. Aubert *et al.* (*BABAR* Collaboration), Phys. Rev. Lett. **98**, 051801 (2007).
[13] B. Aubert *et al.* (*BABAR* Collaboration), Phys. Rev. D **78**, 092008 (2008).
[14] P. del Amo Sanchez *et al.* (*BABAR* Collaboration), Phys. Rev. D **83**, 051101 (2011).
[15] J. Zhang *et al.* (Belle Collaboration), Phys. Rev. Lett. **95**, 141801 (2005).
[16] B. Aubert *et al.* (*BABAR* Collaboration), Phys. Rev. Lett. **97**, 201801 (2006).
[17] R. Aaij *et al.* (LHCb Collaboration), Phys. Rev. Lett. **110**, 241802 (2013).
[18] T. Aaltonen *et al.* (CDF Collaboration), Phys. Rev. Lett. **107**, 261802 (2011).
[19] R. Aaij *et al.* (LHCb Collaboration), Phys. Lett. B **713**, 369 (2012).
[20] R. Aaij *et al.* (LHCb Collaboration), JINST **3**, S08005 (2008).
[21] R. Arink *et al.*, JINST **9**, P01002 (2014).
[22] M. Adinolfi *et al.*, Eur. Phys. J. C **73**, 2431 (2013).
[23] R. Aaij *et al.*, JINST **8**, P04022 (2013).
[24] V. V. Gligorov and M. Williams, JINST **8**, P02013 (2013).
[25] T. Sjöstrand, S. Mrenna, and P. Skands, J. High Energy Phys. 05 (2006) 026; , Comput. Phys. Commun. **178**, 852 (2008).
[26] I. Belyaev *et al.*, in *Nuclear Science Symposium Conference Record (NSS/MIC) IEEE, Knoxville, TN, 2010* (IEEE, 2010), p. 1155
[27] D. J. Lange, Nucl. Instrum. Methods Phys. Res., Sect. A **462**, 152 (2001).
[28] P. Golonka and Z. Was, Eur. Phys. J. C **45**, 97 (2006).
[29] J. Allison *et al.* (GEANT4 Collaboration), IEEE Trans. Nucl. Sci. **53**, 270 (2006); S. Agostinelli *et al.* (GEANT4 Collaboration), Nucl. Instrum. Methods Phys. Res., Sect. A **506**, 250 (2003).
[30] M. Clemencic, G. Corti, S. Easo, C. R. Jones, S. Miglioranzi, M. Pappagallo, and P. Robbe, J. Phys. Conf. Ser. **331**, 032023 (2011).
[31] J. Beringer *et al.* (Particle Data Group), Phys. Rev. D **86**, 010001 (2012).
[32] L. Breiman, J. H. Friedman, R. A. Olshen, and C. J. Stone, *Classification and Regression Trees* (Wadsworth International Group, Belmont, CA, 1984).
[33] R. E. Schapire and Y. Freund, J. Comput. Syst. Sci. **55**, 119 (1997).
[34] T. Skwarnicki, Ph.D. thesis, Institute of Nuclear Physics, Krakow, 1986 [Report No. DESY-F31-86-02].
[35] B. Bhattacharya, A. Datta, M. Duraisamy, and D. London, Phys. Rev. D **88**, 016007 (2013).
[36] T. du Pree, Ph.D. thesis, Nikhef, Amsterdam, The Netherlands, CERN-THESIS-2010-124.
[37] R. Aaij *et al.* (LHCb Collaboration), arXiv:1407.5873.
[38] R. Aaij *et al.* (LHCb Collaboration), Report No. LHCb-CONF-2012-033.
[39] R. Aaij *et al.* (LHCb Collaboration), Report No. LHCb-CONF-2012-026.
[40] G. A. Krocker, Ph.D. thesis, Heidelberg University, Heidelberg, Germany, CERN-THESIS-2013-213.
[41] M. Pivk and F. R. Le Diberder, Nucl. Instrum. Methods Phys. Res., Sect. A **555**, 356 (2005).
[42] Y. Xie, arXiv:0905.0724.
[43] R. Aaij *et al.* (LHCb Collaboration), New J. Phys. **15**, 053021 (2013).
[44] R. Aaij *et al.* (LHCb Collaboration), Phys. Lett. B **709**, 50 (2012).
[45] A. Ali, G. Kramer, Y. Li, C.-D. Lü, Y.-L. Shen, W. Wang, and Y.-M. Wang, Phys. Rev. D **76**, 074018 (2007).

R. Aaij,[41] B. Adeva,[37] M. Adinolfi,[46] A. Affolder,[52] Z. Ajaltouni,[5] S. Akar,[6] J. Albrecht,[9] F. Alessio,[38] M. Alexander,[51] S. Ali,[41] G. Alkhazov,[30] P. Alvarez Cartelle,[37] A. A. Alves Jr,[25,38] S. Amato,[2] S. Amerio,[22] Y. Amhis,[7] L. An,[3] L. Anderlini,[17,a] J. Anderson,[40] R. Andreassen,[57] M. Andreotti,[16,b] J. E. Andrews,[58] R. B. Appleby,[54] O. Aquines Gutierrez,[10] F. Archilli,[38] A. Artamonov,[35] M. Artuso,[59] E. Aslanides,[6] G. Auriemma,[25,c] M. Baalouch,[5] S. Bachmann,[11] J. J. Back,[48] A. Badalov,[36] V. Balagura,[31] W. Baldini,[16] R. J. Barlow,[54] C. Barschel,[38] S. Barsuk,[7] W. Barter,[47] V. Batozskaya,[28] V. Battista,[39] A. Bay,[39] L. Beaucourt,[4] J. Beddow,[51] F. Bedeschi,[23] I. Bediaga,[1] S. Belogurov,[31] K. Belous,[35] I. Belyaev,[31] E. Ben-Haim,[8] G. Bencivenni,[18] S. Benson,[38] J. Benton,[46] A. Berezhnoy,[32] R. Bernet,[40] M.-O. Bettler,[47] M. van Beuzekom,[41] A. Bien,[11] S. Bifani,[45] T. Bird,[54] A. Bizzeti,[17,d] P. M. Bjørnstad,[54] T. Blake,[48] F. Blanc,[39] J. Blouw,[10] S. Blusk,[59] V. Bocci,[25] A. Bondar,[34] N. Bondar,[30,38] W. Bonivento,[15,38] S. Borghi,[54] A. Borgia,[59]

M. Borsato,[7] T. J. V. Bowcock,[52] E. Bowen,[40] C. Bozzi,[16] T. Brambach,[9] J. van den Brand,[42] J. Bressieux,[39] D. Brett,[54] M. Britsch,[10] T. Britton,[59] J. Brodzicka,[54] N. H. Brook,[46] H. Brown,[52] A. Bursche,[40] G. Busetto,[22,e] J. Buytaert,[38] S. Cadeddu,[15] R. Calabrese,[16,b] M. Calvi,[20,f] M. Calvo Gomez,[36,g] P. Campana,[18,38] D. Campora Perez,[38] A. Carbone,[14,h] G. Carboni,[24,i] R. Cardinale,[19,38,j] A. Cardini,[15] L. Carson,[50] K. Carvalho Akiba,[2] G. Casse,[52] L. Cassina,[20] L. Castillo Garcia,[38] M. Cattaneo,[38] Ch. Cauet,[9] R. Cenci,[58] M. Charles,[8] Ph. Charpentier,[38] S. Chen,[54] S.-F. Cheung,[55] N. Chiapolini,[40] M. Chrzaszcz,[40,26] K. Ciba,[38] X. Cid Vidal,[38] G. Ciezarek,[53] P. E. L. Clarke,[50] M. Clemencic,[38] H. V. Cliff,[47] J. Closier,[38] V. Coco,[38] J. Cogan,[6] E. Cogneras,[5] P. Collins,[38] A. Comerma-Montells,[11] A. Contu,[15] A. Cook,[46] M. Coombes,[46] S. Coquereau,[8] G. Corti,[38] M. Corvo,[16,b] I. Counts,[56] B. Couturier,[38] G. A. Cowan,[50] D. C. Craik,[48] M. Cruz Torres,[60] S. Cunliffe,[53] R. Currie,[50] C. D'Ambrosio,[38] J. Dalseno,[46] P. David,[8] P. N. Y. David,[41] A. Davis,[57] K. De Bruyn,[41] S. De Capua,[54] M. De Cian,[11] J. M. De Miranda,[1] L. De Paula,[2] W. De Silva,[57] P. De Simone,[18] D. Decamp,[4] M. Deckenhoff,[9] L. Del Buono,[8] N. Déléage,[4] D. Derkach,[55] O. Deschamps,[5] F. Dettori,[38] A. Di Canto,[38] H. Dijkstra,[38] S. Donleavy,[52] F. Dordei,[11] M. Dorigo,[39] A. Dosil Suárez,[37] D. Dossett,[48] A. Dovbnya,[43] K. Dreimanis,[52] G. Dujany,[54] F. Dupertuis,[39] P. Durante,[38] R. Dzhelyadin,[35] A. Dziurda,[26] A. Dzyuba,[30] S. Easo,[49,38] U. Egede,[53] V. Egorychev,[31] S. Eidelman,[34] S. Eisenhardt,[50] U. Eitschberger,[9] R. Ekelhof,[9] L. Eklund,[51,38] I. El Rifai,[5] Ch. Elsasser,[40] S. Ely,[59] S. Esen,[11] H.-M. Evans,[47] T. Evans,[55] A. Falabella,[14] C. Färber,[11] C. Farinelli,[41] N. Farley,[45] S. Farry,[52] RF Fay,[52] D. Ferguson,[50] V. Fernandez Albor,[37] F. Ferreira Rodrigues,[1] M. Ferro-Luzzi,[38] S. Filippov,[33] M. Fiore,[16,b] M. Fiorini,[16,b] M. Firlej,[27] C. Fitzpatrick,[38] T. Fiutowski,[27] M. Fontana,[10] F. Fontanelli,[19,j] R. Forty,[38] O. Francisco,[2] M. Frank,[38] C. Frei,[38] M. Frosini,[17,38,a] J. Fu,[21,38] E. Furfaro,[24,i] A. Gallas Torreira,[37] D. Galli,[14,h] S. Gallorini,[22] S. Gambetta,[19,j] M. Gandelman,[2] P. Gandini,[59] Y. Gao,[3] J. García Pardiñas,[37] J. Garofoli,[59] J. Garra Tico,[47] L. Garrido,[36] C. Gaspar,[38] R. Gauld,[55] L. Gavardi,[9] G. Gavrilov,[30] E. Gersabeck,[11] M. Gersabeck,[54] T. Gershon,[48] Ph. Ghez,[4] A. Gianelle,[22] S. Giani',[39] V. Gibson,[47] L. Giubega,[29] V. V. Gligorov,[38] C. Göbel,[60] D. Golubkov,[31] A. Golutvin,[53,31,38] A. Gomes,[1,k] H. Gordon,[38] C. Gotti,[20] M. Grabalosa Gándara,[5] R. Graciani Diaz,[36] L. A. Granado Cardoso,[38] E. Graugés,[36] G. Graziani,[17] A. Grecu,[29] E. Greening,[55] S. Gregson,[47] P. Griffith,[45] L. Grillo,[11] O. Grünberg,[62] B. Gui,[59] E. Gushchin,[33] Yu. Guz,[35,38] T. Gys,[38] C. Hadjivasiliou,[59] G. Haefeli,[39] C. Haen,[38] S. C. Haines,[47] S. Hall,[53] B. Hamilton,[58] T. Hampson,[46] X. Han,[11] S. Hansmann-Menzemer,[11] N. Harnew,[55] S. T. Harnew,[46] J. Harrison,[54] J. He,[38] T. Head,[38] V. Heijne,[41] K. Hennessy,[52] P. Henrard,[5] L. Henry,[8] J. A. Hernando Morata,[37] E. van Herwijnen,[38] M. Heß,[62] A. Hicheur,[1] D. Hill,[55] M. Hoballah,[5] C. Hombach,[54] W. Hulsbergen,[41] P. Hunt,[55] N. Hussain,[55] D. Hutchcroft,[52] D. Hynds,[51] M. Idzik,[27] P. Ilten,[56] R. Jacobsson,[38] A. Jaeger,[11] J. Jalocha,[55] E. Jans,[41] P. Jaton,[39] A. Jawahery,[58] F. Jing,[3] M. John,[55] D. Johnson,[55] C. R. Jones,[47] C. Joram,[38] B. Jost,[38] N. Jurik,[59] M. Kaballo,[9] S. Kandybei,[43] W. Kanso,[6] M. Karacson,[38] T. M. Karbach,[38] S. Karodia,[51] M. Kelsey,[59] I. R. Kenyon,[45] T. Ketel,[42] B. Khanji,[20] C. Khurewathanakul,[39] S. Klaver,[54] K. Klimaszewski,[28] O. Kochebina,[7] M. Kolpin,[11] I. Komarov,[39] R. F. Koopman,[42] P. Koppenburg,[41,38] M. Korolev,[32] A. Kozlinskiy,[41] L. Kravchuk,[33] K. Kreplin,[11] M. Kreps,[48] G. Krocker,[11] P. Krokovny,[34] F. Kruse,[9] W. Kucewicz,[26,l] M. Kucharczyk,[20,26,38,f] V. Kudryavtsev,[34] K. Kurek,[28] T. Kvaratskheliya,[31] V. N. La Thi,[39] D. Lacarrere,[38] G. Lafferty,[54] A. Lai,[15] D. Lambert,[50] R. W. Lambert,[42] G. Lanfranchi,[18] C. Langenbruch,[48] B. Langhans,[38] T. Latham,[48] C. Lazzeroni,[45] R. Le Gac,[6] J. van Leerdam,[41] J.-P. Lees,[4] R. Lefèvre,[5] A. Leflat,[32] J. Lefrançois,[7] S. Leo,[23] O. Leroy,[6] T. Lesiak,[26] B. Leverington,[11] Y. Li,[3] T. Likhomanenko,[63] M. Liles,[52] R. Lindner,[38] C. Linn,[38] F. Lionetto,[40] B. Liu,[15] G. Liu,[38] S. Lohn,[38] I. Longstaff,[51] J. H. Lopes,[2] N. Lopez-March,[39] P. Lowdon,[40] H. Lu,[3] D. Lucchesi,[22,e] H. Luo,[50] A. Lupato,[22] E. Luppi,[16,b] O. Lupton,[55] F. Machefert,[7] I. V. Machikhiliyan,[31] F. Maciuc,[29] O. Maev,[30] S. Malde,[55] G. Manca,[15,m] G. Mancinelli,[6] J. Maratas,[5] J. F. Marchand,[4] U. Marconi,[14] C. Marin Benito,[36] P. Marino,[23,n] R. Märki,[39] J. Marks,[11] G. Martellotti,[25] A. Martens,[8] A. Martín Sánchez,[7] M. Martinelli,[41] D. Martinez Santos,[42] F. Martinez Vidal,[64] D. Martins Tostes,[2] A. Massafferri,[1] R. Matev,[38] Z. Mathe,[38] C. Matteuzzi,[20] A. Mazurov,[16,b] M. McCann,[53] J. McCarthy,[45] A. McNab,[54] R. McNulty,[12] B. McSkelly,[52] B. Meadows,[57] F. Meier,[9] M. Meissner,[11] M. Merk,[41] D. A. Milanes,[8] M.-N. Minard,[4] N. Moggi,[14] J. Molina Rodriguez,[60] S. Monteil,[5] M. Morandin,[22] P. Morawski,[27] A. Mordà,[6] M. J. Morello,[23,n] J. Moron,[27] A.-B. Morris,[50] R. Mountain,[59] F. Muheim,[50] K. Müller,[40] M. Mussini,[14] B. Muster,[39] P. Naik,[46] T. Nakada,[39] R. Nandakumar,[49] I. Nasteva,[2] M. Needham,[50] N. Neri,[21] S. Neubert,[38] N. Neufeld,[38] M. Neuner,[11] A. D. Nguyen,[39] T. D. Nguyen,[39] C. Nguyen-Mau,[39,o] M. Nicol,[7] V. Niess,[5] R. Niet,[9] N. Nikitin,[32] T. Nikodem,[11] A. Novoselov,[35] D. P. O'Hanlon,[48] A. Oblakowska-Mucha,[27] V. Obraztsov,[35] S. Oggero,[41] S. Ogilvy,[51] O. Okhrimenko,[44] R. Oldeman,[15,m] G. Onderwater,[65] M. Orlandea,[29] J. M. Otalora Goicochea,[2] P. Owen,[53] A. Oyanguren,[64] B. K. Pal,[59] A. Palano,[13,p] F. Palombo,[21,q] M. Palutan,[18] J. Panman,[38] A. Papanestis,[49,38] M. Pappagallo,[51] C. Parkes,[54] C. J. Parkinson,[9,45]

G. Passaleva,[17] G. D. Patel,[52] M. Patel,[53] C. Patrignani,[19,j] A. Pazos Alvarez,[37] A. Pearce,[54] A. Pellegrino,[41] M. Pepe Altarelli,[38] S. Perazzini,[14,h] E. Perez Trigo,[37] P. Perret,[5] M. Perrin-Terrin,[6] L. Pescatore,[45] E. Pesen,[66] K. Petridis,[53] A. Petrolini,[19,j] E. Picatoste Olloqui,[36] B. Pietrzyk,[4] T. Pilař,[48] D. Pinci,[25] A. Pistone,[19] S. Playfer,[50] M. Plo Casasus,[37] F. Polci,[8] A. Poluektov,[48,34] E. Polycarpo,[2] A. Popov,[35] D. Popov,[10] B. Popovici,[29] C. Potterat,[2] E. Price,[46] J. Prisciandaro,[39] A. Pritchard,[52] C. Prouve,[46] V. Pugatch,[44] A. Puig Navarro,[39] G. Punzi,[23,r] W. Qian,[4] B. Rachwal,[26] J. H. Rademacker,[46] B. Rakotomiaramanana,[39] M. Rama,[18] M. S. Rangel,[2] I. Raniuk,[43] N. Rauschmayr,[38] G. Raven,[42] S. Reichert,[54] M. M. Reid,[48] A. C. dos Reis,[1] S. Ricciardi,[49] S. Richards,[46] M. Rihl,[38] K. Rinnert,[52] V. Rives Molina,[36] D. A. Roa Romero,[5] P. Robbe,[7] A. B. Rodrigues,[1] E. Rodrigues,[54] P. Rodriguez Perez,[54] S. Roiser,[38] V. Romanovsky,[35] A. Romero Vidal,[37] M. Rotondo,[22] J. Rouvinet,[39] T. Ruf,[38] F. Ruffini,[23] H. Ruiz,[36] P. Ruiz Valls,[64] J. J. Saborido Silva,[37] N. Sagidova,[30] P. Sail,[51] B. Saitta,[15,m] V. Salustino Guimaraes,[2] C. Sanchez Mayordomo,[64] B. Sanmartin Sedes,[37] R. Santacesaria,[25] C. Santamarina Rios,[37] E. Santovetti,[24,i] A. Sarti,[18,s] C. Satriano,[25,c] A. Satta,[24] D. M. Saunders,[46] M. Savrie,[16,b] D. Savrina,[31,32] M. Schiller,[42] H. Schindler,[38] M. Schlupp,[9] M. Schmelling,[10] B. Schmidt,[38] O. Schneider,[39] A. Schopper,[38] M.-H. Schune,[7] R. Schwemmer,[38] B. Sciascia,[18] A. Sciubba,[25] M. Seco,[37] A. Semennikov,[31] I. Sepp,[53] N. Serra,[40] J. Serrano,[6] L. Sestini,[22] P. Seyfert,[11] M. Shapkin,[35] I. Shapoval,[16,43,b] Y. Shcheglov,[30] T. Shears,[52] L. Shekhtman,[34] V. Shevchenko,[63] A. Shires,[9] R. Silva Coutinho,[48] G. Simi,[22] M. Sirendi,[47] N. Skidmore,[46] T. Skwarnicki,[59] N. A. Smith,[52] E. Smith,[55,49] E. Smith,[53] J. Smith,[47] M. Smith,[54] H. Snoek,[41] M. D. Sokoloff,[57] F. J. P. Soler,[51] F. Soomro,[39] D. Souza,[46] B. Souza De Paula,[2] B. Spaan,[9] A. Sparkes,[50] P. Spradlin,[51] S. Sridharan,[38] F. Stagni,[38] M. Stahl,[11] S. Stahl,[11] O. Steinkamp,[40] O. Stenyakin,[35] S. Stevenson,[55] S. Stoica,[29] S. Stone,[59] B. Storaci,[40] S. Stracka,[23,38] M. Straticiuc,[29] U. Straumann,[40] R. Stroili,[22] V. K. Subbiah,[38] L. Sun,[57] W. Sutcliffe,[53] K. Swientek,[27] S. Swientek,[9] V. Syropoulos,[42] M. Szczekowski,[28] P. Szczypka,[39,38] D. Szilard,[2] T. Szumlak,[27] S. T'Jampens,[4] M. Teklishyn,[7] G. Tellarini,[16,b] F. Teubert,[38] C. Thomas,[55] E. Thomas,[38] J. van Tilburg,[41] V. Tisserand,[4] M. Tobin,[39] S. Tolk,[42] L. Tomassetti,[16,b] D. Tonelli,[38] S. Topp-Joergensen,[55] N. Torr,[55] E. Tournefier,[4] S. Tourneur,[39] M. T. Tran,[39] M. Tresch,[40] A. Tsaregorodtsev,[6] P. Tsopelas,[41] N. Tuning,[41] M. Ubeda Garcia,[38] A. Ukleja,[28] A. Ustyuzhanin,[63] U. Uwer,[11] V. Vagnoni,[14] G. Valenti,[14] A. Vallier,[7] R. Vazquez Gomez,[18] P. Vazquez Regueiro,[37] C. Vázquez Sierra,[37] S. Vecchi,[16] J. J. Velthuis,[46] M. Veltri,[17,t] G. Veneziano,[39] M. Vesterinen,[11] B. Viaud,[7] D. Vieira,[2] M. Vieites Diaz,[37] X. Vilasis-Cardona,[36,g] A. Vollhardt,[40] D. Volyanskyy,[10] D. Voong,[46] A. Vorobyev,[30] V. Vorobyev,[34] C. Voß,[62] H. Voss,[10] J. A. de Vries,[41] R. Waldi,[62] C. Wallace,[48] R. Wallace,[12] J. Walsh,[23] S. Wandernoth,[11] J. Wang,[59] D. R. Ward,[47] N. K. Watson,[45] D. Websdale,[53] M. Whitehead,[48] J. Wicht,[38] D. Wiedner,[11] G. Wilkinson,[55] M. P. Williams,[45] M. Williams,[56] F. F. Wilson,[49] J. Wimberley,[58] J. Wishahi,[9] W. Wislicki,[28] M. Witek,[26] G. Wormser,[7] S. A. Wotton,[47] S. Wright,[47] S. Wu,[3] K. Wyllie,[38] Y. Xie,[61] Z. Xing,[59] Z. Xu,[39] Z. Yang,[3] X. Yuan,[3] O. Yushchenko,[35] M. Zangoli,[14] M. Zavertyaev,[10,u] L. Zhang,[59] W. C. Zhang,[12] Y. Zhang,[3] A. Zhelezov,[11] A. Zhokhov,[31] L. Zhong[3] and A. Zvyagin[38]

(LHCb Collaboration)

[1]*Centro Brasileiro de Pesquisas Físicas (CBPF), Rio de Janeiro, Brazil*
[2]*Universidade Federal do Rio de Janeiro (UFRJ), Rio de Janeiro, Brazil*
[3]*Center for High Energy Physics, Tsinghua University, Beijing, China*
[4]*LAPP, Université de Savoie, CNRS/IN2P3, Annecy-Le-Vieux, France*
[5]*Clermont Université, Université Blaise Pascal, CNRS/IN2P3, LPC, Clermont-Ferrand, France*
[6]*CPPM, Aix-Marseille Université, CNRS/IN2P3, Marseille, France*
[7]*LAL, Université Paris-Sud, CNRS/IN2P3, Orsay, France*
[8]*LPNHE, Université Pierre et Marie Curie, Université Paris Diderot, CNRS/IN2P3, Paris, France*
[9]*Fakultät Physik, Technische Universität Dortmund, Dortmund, Germany*
[10]*Max-Planck-Institut für Kernphysik (MPIK), Heidelberg, Germany*
[11]*Physikalisches Institut, Ruprecht-Karls-Universität Heidelberg, Heidelberg, Germany*
[12]*School of Physics, University College Dublin, Dublin, Ireland*
[13]*Sezione INFN di Bari, Bari, Italy*
[14]*Sezione INFN di Bologna, Bologna, Italy*
[15]*Sezione INFN di Cagliari, Cagliari, Italy*
[16]*Sezione INFN di Ferrara, Ferrara, Italy*
[17]*Sezione INFN di Firenze, Firenze, Italy*
[18]*Laboratori Nazionali dell'INFN di Frascati, Frascati, Italy*
[19]*Sezione INFN di Genova, Genova, Italy*

[20]*Sezione INFN di Milano Bicocca, Milano, Italy*
[21]*Sezione INFN di Milano, Milano, Italy*
[22]*Sezione INFN di Padova, Padova, Italy*
[23]*Sezione INFN di Pisa, Pisa, Italy*
[24]*Sezione INFN di Roma Tor Vergata, Roma, Italy*
[25]*Sezione INFN di Roma La Sapienza, Roma, Italy*
[26]*Henryk Niewodniczanski Institute of Nuclear Physics Polish Academy of Sciences, Kraków, Poland*
[27]*AGH-University of Science and Technology, Faculty of Physics and Applied Computer Science, Kraków, Poland*
[28]*National Center for Nuclear Research (NCBJ), Warsaw, Poland*
[29]*Horia Hulubei National Institute of Physics and Nuclear Engineering, Bucharest-Magurele, Romania*
[30]*Petersburg Nuclear Physics Institute (PNPI), Gatchina, Russia*
[31]*Institute of Theoretical and Experimental Physics (ITEP), Moscow, Russia*
[32]*Institute of Nuclear Physics, Moscow State University (SINP MSU), Moscow, Russia*
[33]*Institute for Nuclear Research of the Russian Academy of Sciences (INR RAN), Moscow, Russia*
[34]*Budker Institute of Nuclear Physics (SB RAS) and Novosibirsk State University, Novosibirsk, Russia*
[35]*Institute for High Energy Physics (IHEP), Protvino, Russia*
[36]*Universitat de Barcelona, Barcelona, Spain*
[37]*Universidad de Santiago de Compostela, Santiago de Compostela, Spain*
[38]*European Organization for Nuclear Research (CERN), Geneva, Switzerland*
[39]*Ecole Polytechnique Fédérale de Lausanne (EPFL), Lausanne, Switzerland*
[40]*Physik-Institut, Universität Zürich, Zürich, Switzerland*
[41]*Nikhef National Institute for Subatomic Physics, Amsterdam, The Netherlands*
[42]*Nikhef National Institute for Subatomic Physics and VU University Amsterdam, Amsterdam, The Netherlands*
[43]*NSC Kharkiv Institute of Physics and Technology (NSC KIPT), Kharkiv, Ukraine*
[44]*Institute for Nuclear Research of the National Academy of Sciences (KINR), Kyiv, Ukraine*
[45]*University of Birmingham, Birmingham, United Kingdom*
[46]*H.H. Wills Physics Laboratory, University of Bristol, Bristol, United Kingdom*
[47]*Cavendish Laboratory, University of Cambridge, Cambridge, United Kingdom*
[48]*Department of Physics, University of Warwick, Coventry, United Kingdom*
[49]*STFC Rutherford Appleton Laboratory, Didcot, United Kingdom*
[50]*School of Physics and Astronomy, University of Edinburgh, Edinburgh, United Kingdom*
[51]*School of Physics and Astronomy, University of Glasgow, Glasgow, United Kingdom*
[52]*Oliver Lodge Laboratory, University of Liverpool, Liverpool, United Kingdom*
[53]*Imperial College London, London, United Kingdom*
[54]*School of Physics and Astronomy, University of Manchester, Manchester, United Kingdom*
[55]*Department of Physics, University of Oxford, Oxford, United Kingdom*
[56]*Massachusetts Institute of Technology, Cambridge, Massachusetts 02139, USA*
[57]*University of Cincinnati, Cincinnati, Ohio 45220, USA*
[58]*University of Maryland, College Park, Maryland 20742, USA*
[59]*Syracuse University, Syracuse, New York 13210, USA*
[60]*Pontifícia Universidade Católica do Rio de Janeiro (PUC-Rio), Rio de Janeiro, Brazil (associated with Institution Universidade Federal do Rio de Janeiro (UFRJ), Rio de Janeiro, Brazil)*
[61]*Institute of Particle Physics, Central China Normal University, Wuhan, Hubei, China (associated with Institution Center for High Energy Physics, Tsinghua University, Beijing, China)*
[62]*Institut für Physik, Universität Rostock, Rostock, Germany (associated with Institution Physikalisches Institut, Ruprecht-Karls-Universität Heidelberg, Heidelberg, Germany)*
[63]*National Research Centre Kurchatov Institute, Moscow, Russia (associated with Institution Institute of Theoretical and Experimental Physics (ITEP), Moscow, Russia)*
[64]*Instituto de Fisica Corpuscular (IFIC), Universitat de Valencia-CSIC, Valencia, Spain (associated with Institution Universitat de Barcelona, Barcelona, Spain)*
[65]*KVI-University of Groningen, Groningen, The Netherlands (associated with Institution Nikhef National Institute for Subatomic Physics, Amsterdam, The Netherlands)*
[66]*Celal Bayar University, Manisa, Turkey (associated with Institution European Organization for Nuclear Research (CERN), Geneva, Switzerland)*

[a]Also at Università di Firenze, Firenze, Italy.
[b]Also at Università di Ferrara, Ferrara, Italy.
[c]Also at Università della Basilicata, Potenza, Italy.

[d]Also at Università di Modena e Reggio Emilia, Modena, Italy.
[e]Also at Università di Padova, Padova, Italy.
[f]Also at Università di Milano Bicocca, Milano, Italy.
[g]Also at LIFAELS, La Salle, Universitat Ramon Llull, Barcelona, Spain.
[h]Also at Università di Bologna, Bologna, Italy.
[i]Also at Università di Roma Tor Vergata, Roma, Italy.
[j]Also at Università di Genova, Genova, Italy.
[k]Also at Universidade Federal do Triângulo Mineiro (UFTM), Uberaba-MG, Brazil.
[l]Also at AGH - University of Science and Technology, Faculty of Computer Science, Electronics and Telecommunications, Kraków, Poland.
[m]Also at Università di Cagliari, Cagliari, Italy.
[n]Also at Scuola Normale Superiore, Pisa, Italy.
[o]Also at Hanoi University of Science, Hanoi, Viet Nam.
[p]Also at Università di Bari, Bari, Italy.
[q]Also at Università degli Studi di Milano, Milano, Italy.
[r]Also at Università di Pisa, Pisa, Italy.
[s]Also at Università di Roma La Sapienza, Roma, Italy.
[t]Also at Università di Urbino, Urbino, Italy.
[u]Also at P.N. Lebedev Physical Institute, Russian Academy of Science (LPI RAS), Moscow, Russia.